

Slopes of Oceanic Basalt Volcanoes

Scott K. Rowland¹ and Harold Garbeil

*Hawaii Institute of Geophysics and Planetology, School of Ocean and Earth Sciences and Technology
University of Hawaii at Manoa, Honolulu*

Digital elevation and slope data have been compiled for 15 basaltic volcanoes in four oceanic hotspot regions that represent a wide morphological spectrum of young basaltic shields. The data for each region were collected by a different remote-sensing technique: interpolation between spot elevations in orthophotoquads (Hawaii); TOPSAR single-pass interferometric radar (western Galapagos); ERS1/2 tandem 1-day repeat-pass radar interferometry (Grand Comoro); and SIR-C 1-day repeat-pass radar interferometry (Réunion). These remotely sensed data provide information about the time-integrated typical activity of each volcano and allow us to assess the spatial and temporal contributions of various constructional and destructional processes to each volcano's present morphology. Gradual slopes ($<5^\circ$) occur where lava and tephra pond within calderas or in the saddles between adjacent volcanoes, as well as where lava deltas coalesce to form coastal plains. Vent concentration zones (axes of rift zones or Galapagos summit platforms) have slopes ranging from 10 to 12°. Differential vertical growth rates between vent concentration zones and adjacent mostly-lava flanks produce steep constructional slopes up to 40°. The steepest slopes (locally approaching 90°) are produced by fluvial erosion, caldera collapse, faulting, and catastrophic avalanches, all of which are usually identifiable. The quantitative study of volcano morphology allows inferences to be made about the nature, location, and magnitude of activity over timescales of 10^0 to 10^4 years, and the relative importance of particular processes in particular settings holds useful information about internal volcanic structure and evolution. The complex spatial and temporal interplay of these slope-forming processes precludes derivation of volcano morphology by numerical modeling of single processes or unidirectional evolutionary schemes. We conclude that the different types of digital elevation data are equally useful for the analysis of volcanic landforms at a scale of a few square kilometers. This is advantageous because future similar work on other volcanoes can proceed as new topographic data become available from other sensors.

¹ Also Hawaii Center for Volcanology, School of Ocean and Earth Science and Technology, University of Hawaii at Manoa, 2525 Correa Rd., Honolulu, Hawaii, 96822, USA

Table 1. Data Types Presented in This Study

Data Type	Remote Sensing Platform	Spatial Resolution	Date Collected	Example in Present Study
single-pass dual antenna radar interferometry	TOPSAR (flown on a DC-8 aircraft)	10 m	May 29, 1993	western Galapagos
dual-pass dual antenna radar interferometry	ERS-1 and ERS-2 satellites flown in tandem (1 day between images)	30 m	November 26 and 27, 1995	Grand Comoro
dual-pass single antenna radar interferometry	Shuttle Imaging Radar-C (SIR-C; 1-day repeat cycle)	25 m	October 1994	Réunion
interpolation of spot elevations	7.5-minute ortho-photoquads (derived from stereo air photos)	interpolated and gridded to 30 m	1977	Hawaii

INTRODUCTION

Basaltic shield volcanoes are usually considered to have gentle, rather monotonous slopes [e.g., *Simkin and Siebert*, 1994] although the Galapagos shields have long been noted as unique [*Williams and McBirney*, 1979]. Various attempts have been made to model basaltic shield morphology with the underlying assumption that a single process or set of evolutionary steps produces the final form (e.g., *Nordlie*, 1973; *Cullen et al.*, 1987]. In detail, however, radial and circumferential variations in slope can be found on all shield volcanoes. Because the morphology of a volcano is an integration of all the destructional and constructional processes that occurred during its history, studying this morphology can provide clues about internal structure and eruption history [e.g., *Moore and Mark*, 1992]. Volcano morphology can be quantified using digital elevation models (DEMs) and is readily visible in shaded relief images. Surface slope provides additional information for analyzing morphological features on parts of individual volcanoes as well as on separate volcanoes.

The rest of this volume focuses on remote sensing of active volcanism. Here we take a longer-term view at the way that constructional and destructional volcanic processes result in particular volcanic morphologies. This is possible because in recent years satellite and aircraft remote sensing techniques have dramatically increased the quantity and quality of digital topographic data from volcanic sites. In particular we present a compilation of topography and slope data for 15 oceanic basalt shield volcanoes using a variety of DEMs (Table 1). Because our data

were derived using various techniques, we are also able to assess the relative utility of these data types for volcano morphology studies. We have made particular use of digital elevation data derived from radar interferometry, in which an interferogram is produced from two synthetic aperture radar (SAR) images collected at nearly identical viewing locations [*Zebker and Goldstein*, 1986]. These images can either be collected simultaneously by a twin antenna (the single-pass technique) or at different times by one or more single antennas (the dual-pass technique).

We present digital elevation data in three forms; shaded relief images, slope images, and graphs of average slope vs. elevation [after *Moore and Mark*, 1992]. The slope at each pixel in the slope images was calculated on the basis of the elevations of the 8 adjacent pixels [*Mouginis-Mark et al.*, 1996]. For each of the 15 volcanoes we collected slope statistics within 100-m elevation intervals and present the data as plots of average slope vs. either actual or normalized (%) elevation. The latter allows easier comparison between volcanoes of different heights. The relative ease with which the data can be manipulated also allows selection of sub-areas within each DEM for analysis of slope statistics; this is important because these volcanoes are not radially symmetric.

DATA SETS

The data for the western Galapagos volcanoes were collected by the TOPSAR single-pass interferometric radar [*Zebker et al.*, 1992; *Evans et al.*, 1992], which utilizes two antennae mounted on a DC-8 aircraft, separated vertically

by ~2.5 m. TOPSAR produces DEMs with 10-m spatial resolution and 1-2 m vertical accuracy on a variety of geological surfaces [Izenberg *et al.* 1996; Rowland *et al.* 1999]. In late 1995 the European Resources Satellites-1 and -2 (ERS-1 and ERS-2) were flown in tandem mode, meaning they were in near-identical orbits separated by a day. The data presented here for Grand Comoro were produced from an interferogram of an ERS-1 scene (26 November) and an ERS-2 scene (27 November). The last four days of the second Shuttle Imaging Radar-C (SIR-C) flight in October 1994 were devoted to single-antenna dual-pass interferometry [Mouginis-Mark, 1995] and provided the data presented here for Piton de la Fournaise.

Compared to older techniques for deriving digital elevation data (see below), interferometry offers the advantage of producing an elevation measurement at every pixel-equivalent location on the ground. Radar's ability to penetrate clouds and darkness also means that elevation data can be gathered where ambient conditions preclude collection of air photos. At present, only a few interferometric DEMs of volcanoes are available, although the Shuttle Radar Topography Mission (SRTM) scheduled for late 1999 will provide single-pass digital elevation data for all of the Earth between 60°N and 54°S at spatial and vertical resolutions of ~30 m and ~16 m, respectively [Zebker *et al.*, 1994; Farr *et al.* 1995]. An additional upcoming topography data set will be produced by the advanced spaceborne thermal and emission radiometer (ASTER), an instrument on the Earth Observing System [Lang and Welch, 1996]. ASTER will use principles of photogrammetry applied to digital images [Panton 1978] to produce 60×60 km DEMs with 15-m spatial resolution [Lang and Welch, 1996; Welch *et al.*, 1998].

Uncertainty in the accuracy of interferometrically derived DEMs arises from a number of sources. Because SAR views the ground at an angle, steep slopes sometimes cast radar shadows, producing blank areas within images. The most obvious examples in the data presented here are in the calderas of the western Galapagos volcanoes. The spatial separation between the points at which the two radar images are collected is termed the baseline. Elevation errors are minimized if the baseline is known accurately and has an optimal length with respect to other parameters of the particular radar system such as wavelength, look angle, etc. For single-pass systems such as TOPSAR, the baseline is known and constant, but structural limitations on the airframe mean that the ~2.5-m-baseline is considerably less than the optimal 150 m [Zebker *et al.*, 1992].

Dual-pass interferometry produces a baseline because the two passes are never identical. Errors in this technique

are due to variations and/or uncertainties in the baseline that arise from navigation uncertainties. Baseline uncertainties produced minor slope distortions in the Grand Comoro DEM (see below). An additional limitation is that any changes in the surface characteristics (e.g., in soil moisture, snow cover, and vegetation canopy) that occur between the times of the two passes make it difficult to correlate the two images on a pixel-by-pixel basis. Finally, the ability of radar to penetrate vegetation is variable and depends on factors such as vegetation density, branch orientation, and vegetation moisture [e.g., Imhoff, 1986]. A DEM in vegetated regions may therefore reflect some level within the leaf canopy rather than the actual ground surface. The upcoming flight of the vegetation canopy lidar (VCL) space mission in 2000 will use a laser to penetrate vegetation canopy to produce 50-cm-wide topographic profiles that will help facilitate vegetation corrections in DEMs.

An older technique for producing digital elevation data involves collecting gridded elevation points from analog data sets such as orthophotoquads, stereo air photos, and topographic maps [USGS, 1990; Moore and Mark, 1992]. These gridded spot elevations are then interpolated and mosaiced to produce a DEM. The data presented here for the 5 volcanoes making up the Island of Hawaii were derived by the U.S. Geological Survey in this manner from 7.5-minute orthophotoquads produced in 1977. The original elevation point spacing was approximately 8.6 m, and the data were resampled to 30-m pixels. They have absolute vertical accuracy of ±7 m [USGS, 1990], but the relative vertical accuracy within an individual quad is considerably better. For our study, individual quads were mosaiced by the Jet Propulsion Laboratory to produce a DEM of the island. Accuracy in this technique is reduced if the original photo data are of poor quality or contain clouds, or if the interpolation is not done carefully. Mosaicking of quads into a DEM as well as mosaicking of the patches that form quads [USGS, 1990] can produce seams in the final DEM.

SLOPE DESCRIPTIONS

Hawaii

Shaded relief and slope images for 5 Hawaiian volcanoes are presented in Figure 1a and Plate 1a, respectively, and Figure 2 presents slope versus elevation data. Mark and Moore [1987] and Moore and Mark [1992] provide detailed discussions and geological interpretations of slope

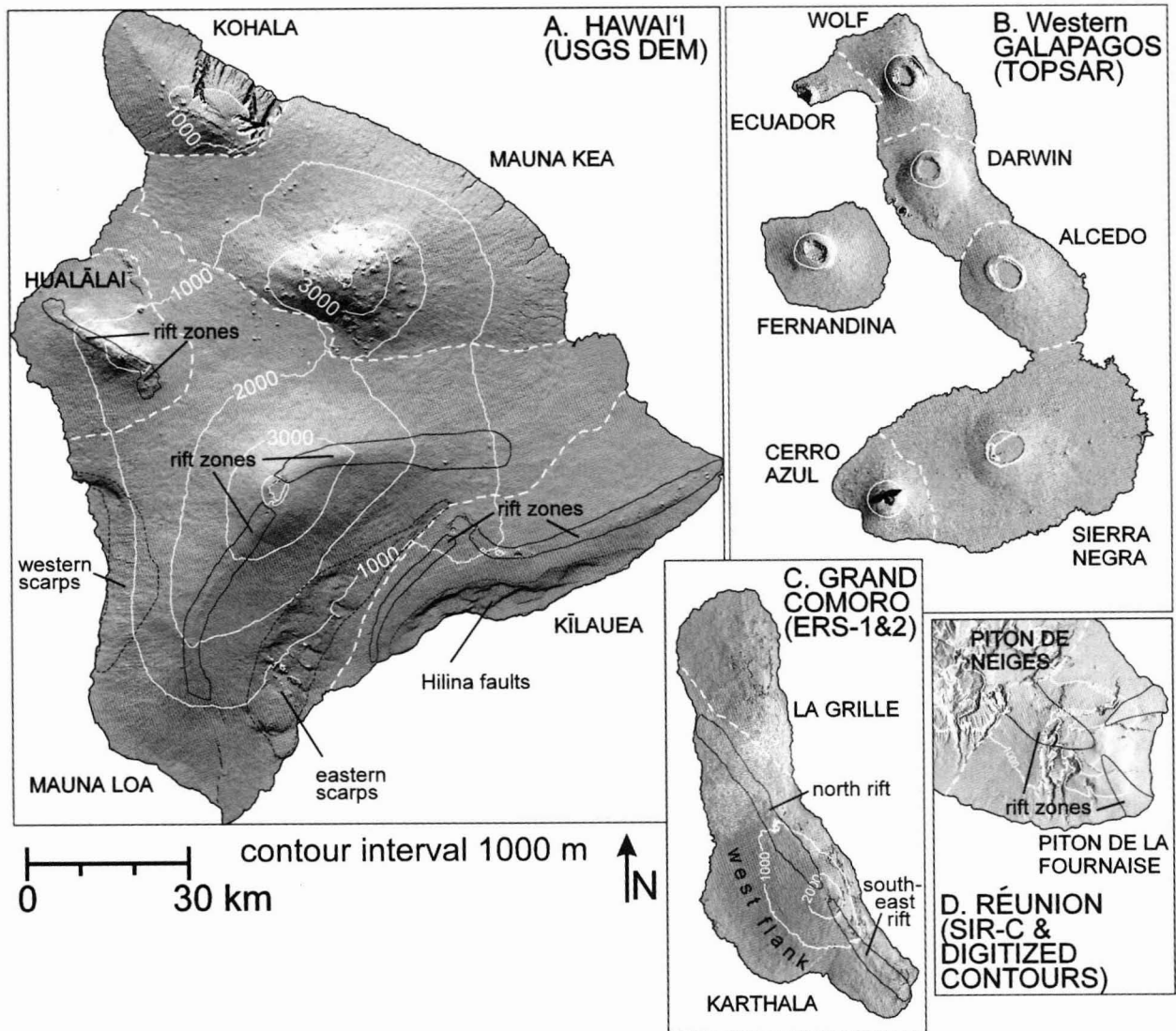


Figure 1. Shaded relief images of DEM data for the 15 volcanoes covered in this study. The Hawaii image (a) has pseudo-illumination from the north; western Galapagos (b), Grand Comoro (c), and Réunion data have pseudo illumination from the east. Dashed white lines indicate volcano boundaries as in Plate 1, black lines indicate volcano-structural features discussed in text. Black areas in Galapagos and Grand Comoro maps are regions of no data owing to radar shadowing or lack of coherence.

regions on these volcanoes, most of which will not be repeated here. Plotting slope versus elevation makes comparison between slope features and geographical features easier (e.g., between Figures 2a, 1a, and Plate 1a). For example, the lowest values of average slope on Mauna Kea occur between 800 and 900 m because of the areal contribution at these elevations by the saddle against Kohala. The lowest elevations of Kilauea and Kohala contain significant slope contributions from steep fault scarps and stream valleys, respectively. Contributions to slopes by various features are presented in Table 2.

Figure 2b plots slope versus percent elevation, with the effects of faults and valleys removed from the Kilauea and Kohala data. Except for Mauna Kea, the volcanoes display relatively constant slopes from the coast to about 50% of their maximum elevations. Average slope values are lower for Mauna Loa and Kilauea, which are still within the most active tholeiite shield-building stage. Average slopes are higher for the three less active volcanoes (Hualalai, Mauna Kea, and Kohala), which are in, or have gone through, the post-shield alkalic stage [e.g., Peterson and Moore, 1987]. Above the 50% elevation level, all the volcanoes except

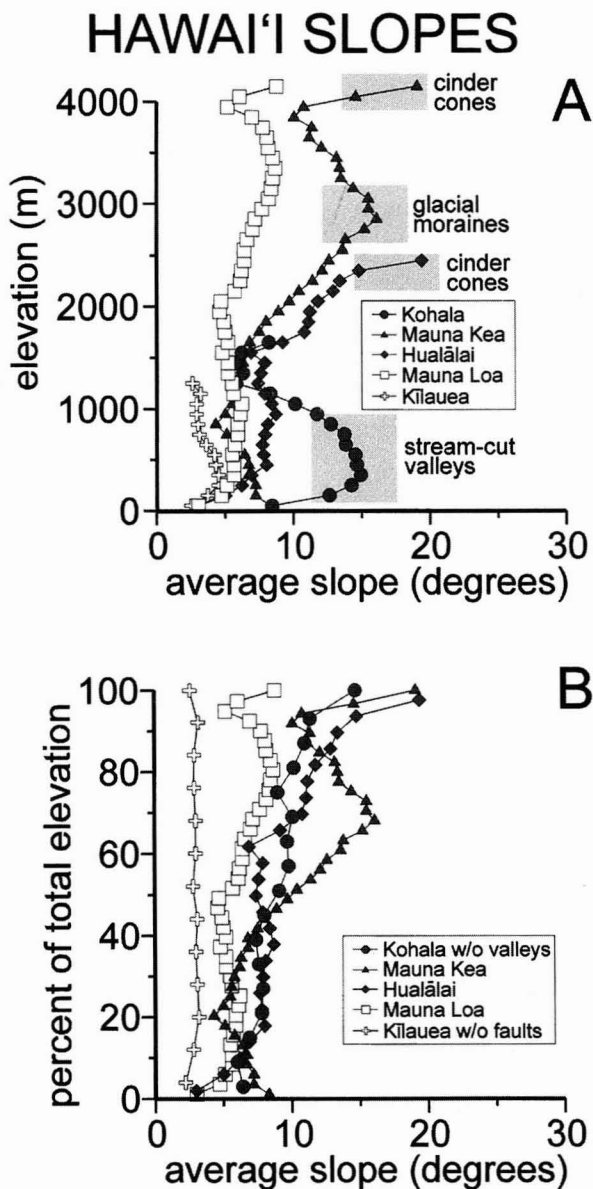


Figure 2. Average slope versus elevation (a) and versus % elevation (b) for the 5 volcanoes of the island of Hawaii. In (a), gray boxes highlight particular geologic features that produce distinct slope effects. In (b), erosional valleys and the Hilina faults have been excluded from analyses for the Kohala and Kilauea data, respectively.

Kilauea steepen with elevation (Table 2B). The two tallest volcanoes, Mauna Kea and Mauna Loa, reach maximum slopes at 70% and 80% of their elevations, respectively, before becoming more gradual higher. The highest elevations of Mauna Kea, Hualalai, and Kohala are dominated by steep-sided cinder cones that produce high average

slopes but these elevations represent only insignificant areas of each volcano. The highest elevation increment on Mauna Loa has a steep contribution from the walls of Mokuaweoweo Caldera but these are likewise areally insignificant.

On Mauna Loa, avalanche scarps contribute about 1° of increased average slope between 100 and 1500 m (Figure 3), but become areally insignificant above 2000 m. The southwest and northeast rift zones are distinct only above about 1500 m, and above 2000 m the average slopes of the rift zone axes are almost 5° less than those of the adjacent east and west flanks (Figure 3). Thus on Mauna Loa, constructional slopes composed exclusively of lava flows (i.e., not along rift zone axes and not including avalanche scars) increase from $\sim 3^\circ$ at the coast to $\sim 5^\circ$ at about 2000 m and then steepen more rapidly to nearly 9° at about 3300 m. Average slope minima correspond to the saddles with Hualalai (~ 1500 m) and Mauna Kea (~ 2000 m), and to the caldera floor (~ 4000 m). The rift zones, with the highest proportions of pyroclastic material, have average slopes $< 7^\circ$ at all elevations. Because the rift zones are relatively narrow, however, clusters of cinder cones can locally dominate (and steepen) the average slopes such as at around 3100 m.

When Hilina Pali faults are not considered, Kilauea (Figure 4) shows slope patterns that are somewhat similar to those of Mauna Loa, although at a nearly constant 3° throughout all elevations they are the lowest whole-volcano slopes for any of the volcanoes in this study. More than 30 large normal fault blocks comprise the Hilina Pali system [Holcomb, 1987], and the fault scarps locally reach 40° . However, the gently sloping upper surfaces of the blocks occupy much larger areas so that average slopes within the Hilina Pali system are less than 8° . The Kilauea rift zones have slopes similar to those of the flanks (without faults) but contain a contribution from pit crater walls at their highest elevations, increasing their average slopes to $\sim 4^\circ$.

Because of their prominent rift zones, Hawaiian volcanoes are not radially symmetric with respect to their slopes (Plate 1a). Near-horizontal regions are found in caldera floors and the saddles between volcanoes. Near-horizontal slopes also occur along 1-10 km-wide stretches of coastline on Hualalai, Mauna Loa, and Kilauea, but these are absent on Mauna Kea and Kohala [Moore and Mark, 1992]. The average slopes along the Mauna Loa and Hualalai rift zone axes are 5° and 7° , respectively, in contrast to the average slopes of the adjacent rift zone flanks of 9° and 16° (which would be steeper if mass-wasting features were considered); the rift zones therefore stand out in the slope data (Plate 1a). A similar relationship occurs on Kohala but the low slopes of the rift zone axis are largely due to a contribution from the floors of graben [Stearns and Macdonald,

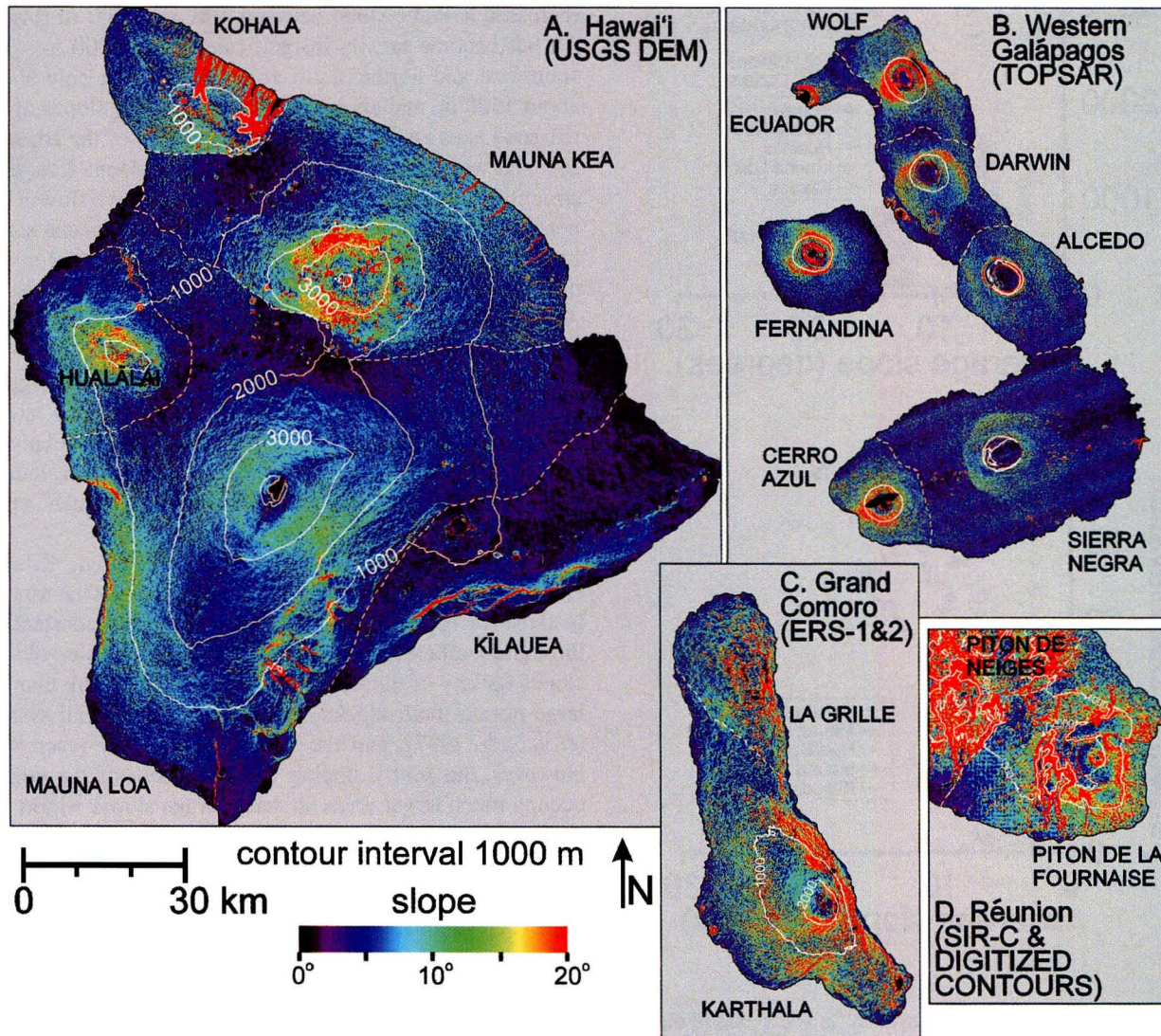


Plate 1. Slope data for the 15 volcanoes covered in this study. Dashed white lines indicate volcano boundaries, in some cases based on distinct changes in slope (see text). Stripes in Galapagos data are artifacts parallel to flight lines. Black areas in Galapagos and Grand Comoro maps are regions of no data owing to radar shadowing or lack of coherence.

Table 2. Slope Features on Hawaiian Volcanoes
(A) Absolute Elevation

Volcano	Elevation Increment (m)	Average Slope (degrees) ^a	Dominant slope modifier
Kohala	0-100	8	flank flows, coastal cliffs
	100-900	12-15	stream-cut valleys on NE flanks
	900-1600	6-8	summit graben, large cinder cones
Mauna Kea	0-700	6-8	stream valley walls, NE coast
	800-1000	4-5	saddle against Kohala
	1000-2600	5-15	increasing concentration of pyroclastic vents ^b
	2600-3100	15-17	terminal moraines ^b
	3100-3800	15-10	tops of moraines, flows ponded between cones
Hualalai	3800-4100	10-20	large cinder cones
	0-100	3-9	lava deltas ^b , increasing concentration of pyroclastic vents ^b
	400-1100	9	buried avalanche scarp(?) ^b
	1100-1500	7-8	saddle with Mauna Loa
Mauna Loa	1500-2400	5-20	increasing concentration of pyroclastic vents ^b
	0-100	3	lava deltas ^b
	100-1900	3-6	slight contribution from avalanche scarps
	1900-2100	5	saddle against Mauna Kea
	2100-3400	5-9	Intrusions, ^c short summit-derived lava flows, ^c buried moraines(?)
	3400-3900	9-5	broad-scale summit subsidence, caldera floor
Kīlauea	3900-4100	5-10	caldera walls
	0-100	3	lava deltas, tops of lowest fault blocks
	100-600	3-5	Hilina faults
	600-1200	3	broad-scale summit subsidence, saddle with Mauna Loa

^anumber order gives the sense of change (if one exists)

^b[Moore and Mark, 1992]

^c[Lipman, 1995]

Table 2. Slope Features on Hawaiian Volcanoes
(B) Normalized Elevation

Volcano	Increment (%)	Average Slope or Slope Range (°)	Change in Slope (%/10% Elevation Increase)
Kohala (without valleys)	0-50	8	0
	50-100	10-15	+1
Mauna Kea	0-20	9-5	-2
	20-70	5-16	+2.2
	70-90	16-10	-3
	90-100	10-20	+10
Hualalai	0-20	3-9	+3
	20-60	9	0
	60-100	8-20	+3
Mauna Loa	0-50	5	0
	50-80	5-9	+1.3
	80-95	9-5	-2.7
	95-100	5-10	+10
Kilauea (without Hilina faults)	0-100	3	0

1946]. The rift zones of Kilauea have average slopes of 3-4° but do not stand out in the slope data because the flanks of the entire volcano are also gradual. When the effects of avalanche scars and valleys are removed, all the Hawaii volcanoes except Kilauea show some degree of upward steepening. Additionally, both Plate 1 and Table 2 show that there is a correlation between the height of a Hawaiian volcano and the number of large-scale slope variations it possesses.

Distinct changes in slope correspond to the boundaries between northern Mauna Kea (gradual) and southern Kohala (steeper) and between northern Mauna Loa (gradual) and southern Mauna Kea (steeper; Plate 1a; *Moore and Mark, 1992*). In contrast, no distinct changes in slope occur between Mauna Loa and Hualalai or between Mauna Loa and Kilauea.

The Western Galapagos

The slopes of the western Galapagos volcanoes have received considerable attention, mainly because they differ from those of Hawaiian volcanoes [e.g., *McBirney and Williams, 1969*]. Figure 1b and Plate 1b present shaded

relief and slope images, respectively, and Figure 5 presents slope and elevation data. The western Galapagos volcanoes can be classified into two groups based on their overall slope characteristics [*Mouginis-Mark et al., 1996*]. Darwin, Alcedo, and Sierra Negra have slopes that increase relatively constantly from ~5° near the coast to 10-12° at about 80% of their elevation, corresponding to changes in slope of 0.7-1.3° per 10% elevation. Above this they are considerably steeper but the areal contribution of these uppermost slopes is minor. In contrast, Wolf, Cerro Azul, and Fernandina steepen from ~5° near the coast to more than 20° by 75% of their height (1.6 to 2.4° per 10%). The volcanoes in the first group have relatively shallow calderas (between 200 and 360 m deep), contrasting with those in the second group (475-920 m deep; *Munro and Rowland [1996]*). These caldera depths are 18-30% and 30-63% of the subaerial heights, respectively. In neither group does the elevation of the caldera floor correspond consistently to any particular outer flank slope feature (Figure 5).

For Fernandina, *Rowland [1996]* defined roughly concentric regions of the volcano from the coast inland that vary with respect to both average slope and the number of

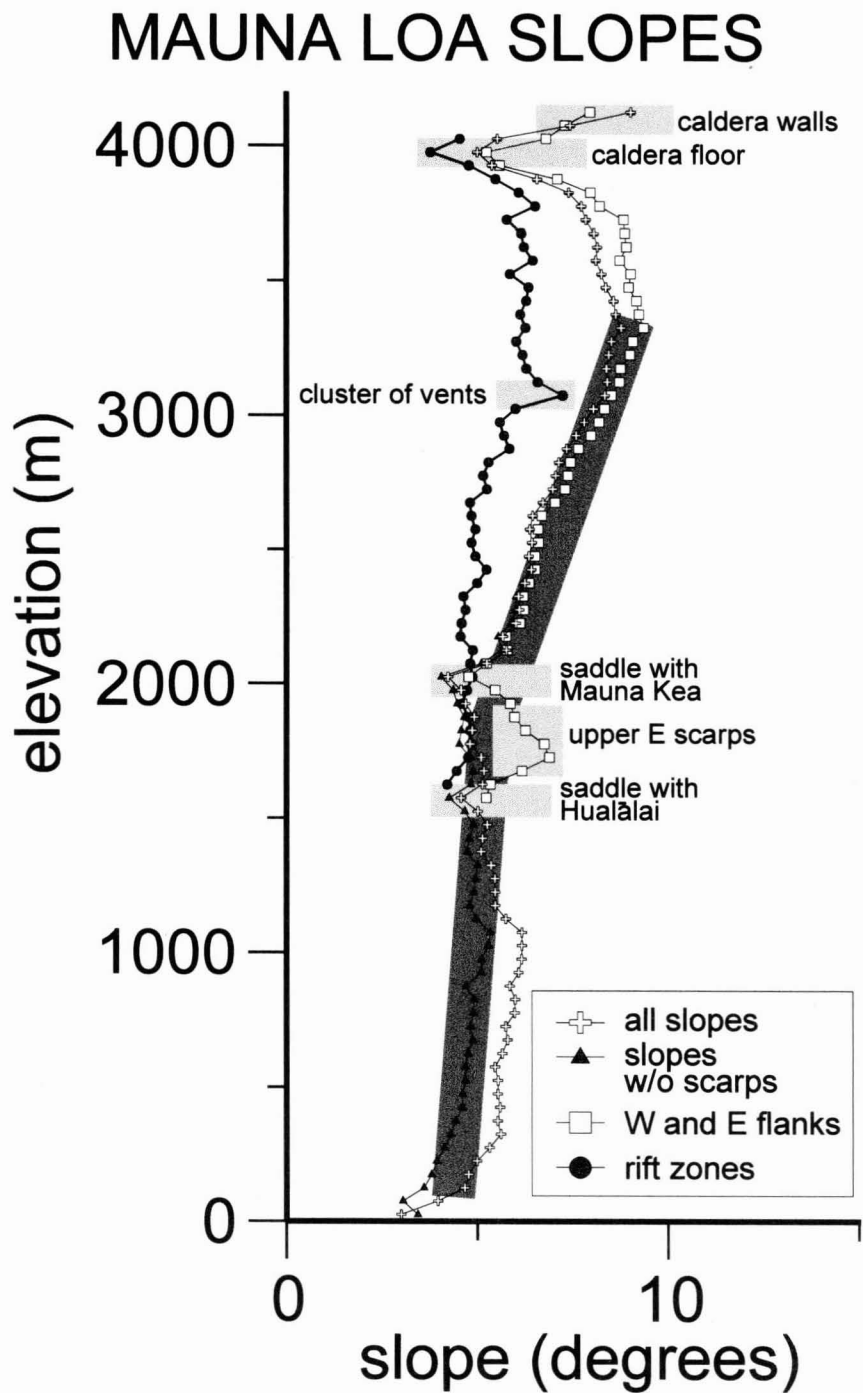


Figure 3. Average slope versus elevation for Mauna Loa. Gray boxes highlight particular geologic features that produce distinct slope effects. Note that masking scarps from the analysis between 100 and 1500 m elevation reduces average slopes by $\sim 1^\circ$. Darkest shading indicates behavior of constructional slopes consisting only of lava (not affected by avalanche scarps and not including rift zones).

KĪLAUEA SLOPES

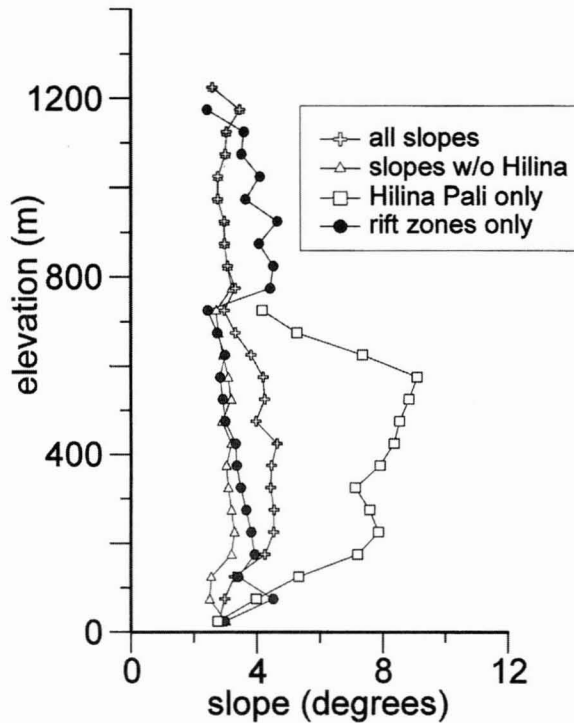


Figure 4. Average slope versus elevation for Kīlauea volcano.

vents/area (Figure 6a; Table 3a). The coastal plain is almost entirely lava and has the lowest average slopes. Within the apron, inland-increasing concentrations of radial vents correspond to inland-increasing average slopes. The steep slopes have few vents whereas the summit platform has the highest vent concentration on the volcano. Rowland [1996] also divided Fernandina into pie-shaped sectors based on vent distributions, the relative ages of lava flows, and slope characteristics (Figure 6a). The variation of average slope with elevation within these sectors is shown in Figure 6b and Table 3b. The lowest elevations in all sectors have gradual slopes, and the north flank is the steepest at all elevations. In the northeast-southeast and south-west sectors, the top of the apron (the inland extent of radial vents) coincides with a distinct increase in slope. The northwest flank shows a gradual increase in slope from the coastline to the caldera rim, corresponding to a relatively constant vent concentration. For all sectors, the average slope of the summit platform is $\sim 10^\circ$.

Figure 6c presents a similar analysis for Wolf volcano, divided into pie-shaped sectors defined by the presence or absence of vent concentrations [Chadwick and Howard,

1991]. The results for Wolf (Figure 6d) are roughly similar to those at Fernandina. Compared to the volcano as a whole, average slopes are lower in the north, west-northwest, and south sectors where radial vents are concentrated (analogous to the northwest flank of Fernandina). Average slopes are greater for the northeast, southwest, and northwest sectors where there are few or no radial vents (analogous to the north flank of Fernandina).

Table 4 tabulates slope region statistics for the 5 volcanoes on Isla Isabela. The patterns are roughly the same as those on Fernandina but there are differences in the percentages of the different slope regions. For example, 70% of Sierra Negra consists of coastal plain whereas only 3% can be considered to be steep slopes.

In general, the Galapagos volcanoes have near-horizontal slopes within calderas, in the saddles between volcanoes, and along coastal plains of varying widths, similar to the Hawaii examples. Also, some Galapagos volcano boundaries correspond to distinct changes in slope whereas others do not. In contrast to Hawaii, distinct summit platforms occur on Fernandina, Cerro Azul, Wolf, and Sierra Negra, and these tend to have gradual average slopes. The steepest slopes (not counting caldera walls and rare flank faults) occur in the regions between these summit platforms and the lower flanks.

Grand Comoro

The island of Grand Comoro, about halfway between Madagascar and Mozambique at $11^\circ 40'S$, $43^\circ 20'E$, consists of the two shield volcanoes Karthala and La Grille [Bachèlery and Coudray, 1993; Figure 1c; Plate 1c]. The morphology of Karthala is somewhat transitional between those of the Hawaiian and Galapagos shields. Similar to Hawaii, rift zones impart a distinct elongation to the plan-view shape. These rift zones are combined with a roughly circular central cone similar to the Galapagos shields in that it contains a significant number of radial vents, although they are relatively evenly distributed from the coastline to the summit and there are no arcuate vents in the summit region [Bachèlery and Coudray, 1993]. Comparison with a topographic map indicates that foreshortening due to baseline uncertainty has caused east-facing slopes to be $2-3^\circ$ too steep and west-facing slopes to be $2-3^\circ$ too gentle in the ERS-1/2-derived DEM of Grand Comoro, but this bias is not sufficient to invalidate the overall slope relationships.

Somewhat discontinuous coastal plains on Karthala have average slopes of $\sim 5^\circ$ and inland the volcano steepens rapidly to $\sim 10^\circ$. The west flank has average slopes that range between 10 and 14° up to ~ 2100 m where a greater

W. GALÁPAGOS SLOPES

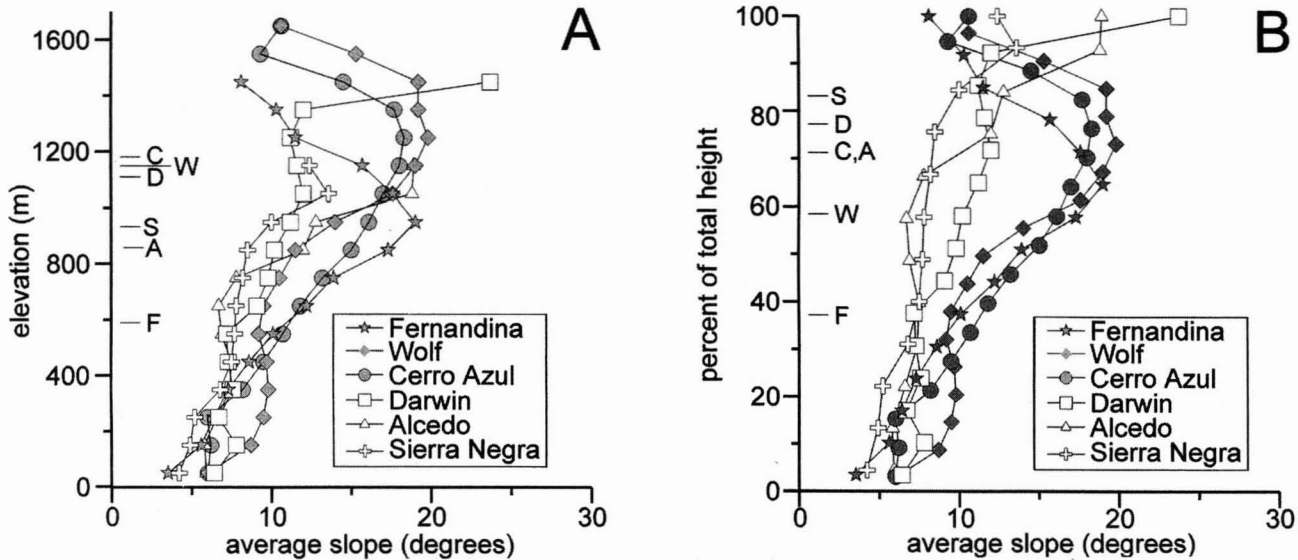


Figure 5. Average slope versus elevation (a) and % elevation (b) for the 6 active shields in the western Galapagos. The two slope/caldera populations defined by *Mouginis-Mark et al.* [1996] are shown in filled (steep outer flanks, deep calderas) and unfilled (gradual outer flanks, shallow calderas) symbols. Letters at left show caldera floor elevations corresponding to each volcano.

number of cinder cones causes an increase. Slopes along the 3-4 km-wide axis of the north rift zone average 4-5° less than those of the adjacent west flank (Figure 7). Clusters of cinder cones [*Bachèlery and Coudray, 1993*] near 800 and 1700 m raise the average north rift zone slopes to 12-13°. The east flank has average slopes in excess of 20°, to a large extent due to numerous avalanche and fault scarps [*Bachèlery and Coudray, 1993*]. Similar to the Hawaii and Galapagos examples, Karthala has gradual slopes along the coast, within the caldera, and in the saddle separating it from LaGrille.

Coastal plains on LaGrille are nearly horizontal whereas the slopes immediately inland steepen abruptly. Average slopes at the highest elevations are dominated by the flanks of numerous large cinder cones. Between Karthala and LaGrille is a relatively distinct change in slope oriented roughly northwest-southeast (interpreted in this study to be the volcano boundary; Plate 1, Figure 1). Slopes southwest of this line are <5°, whereas those to the northeast are ~10°.

Piton de la Fournaise

Piton de la Fournaise (Figure 1d; Plate 1d; Figure 8) forms the southeast part of Réunion Island (21°7.5'S,

55°30'E) and has undergone extensive gradual and catastrophic erosion [e.g., *Duffield et al., 1982*]. Piton de la Fournaise originally grew against the southeast flank of an older, dissected volcano, Piton de Neiges (Figure 8a), and has rebuilt itself against (or within) avalanche scars at least 3 times [*Duffield et al., 1982*]. This geologic history makes slope analyses more straightforward if the volcano is divided into structural sections. Figure 9b presents slope data for the entire volcano with and without valleys and scarps. The two plots are essentially parallel above 900 m, indicating that valleys and scarps comprise relatively constant (but unequal) percentages of the volcano at these elevations. Ignoring the valleys and scarps, slopes increase from ~9° near the coast to ~13° at about 500 m, and maintain this to around 1500 m, the elevation of the caldera. Here the average slopes decrease sharply before they increase again above this to nearly 20°. The highest elevations have gentler slopes that are dominated by the plains of Cafres and Sables, composed of lavas and pyroclasts ponded against Piton de Neiges and an avalanche scarp, respectively.

Figure 9c presents slope data for the next-to-youngest and youngest parts of the edifice, both of which grew within major avalanche scars. The slope data for the next-to-youngest part roughly mimic those for the volcano as a

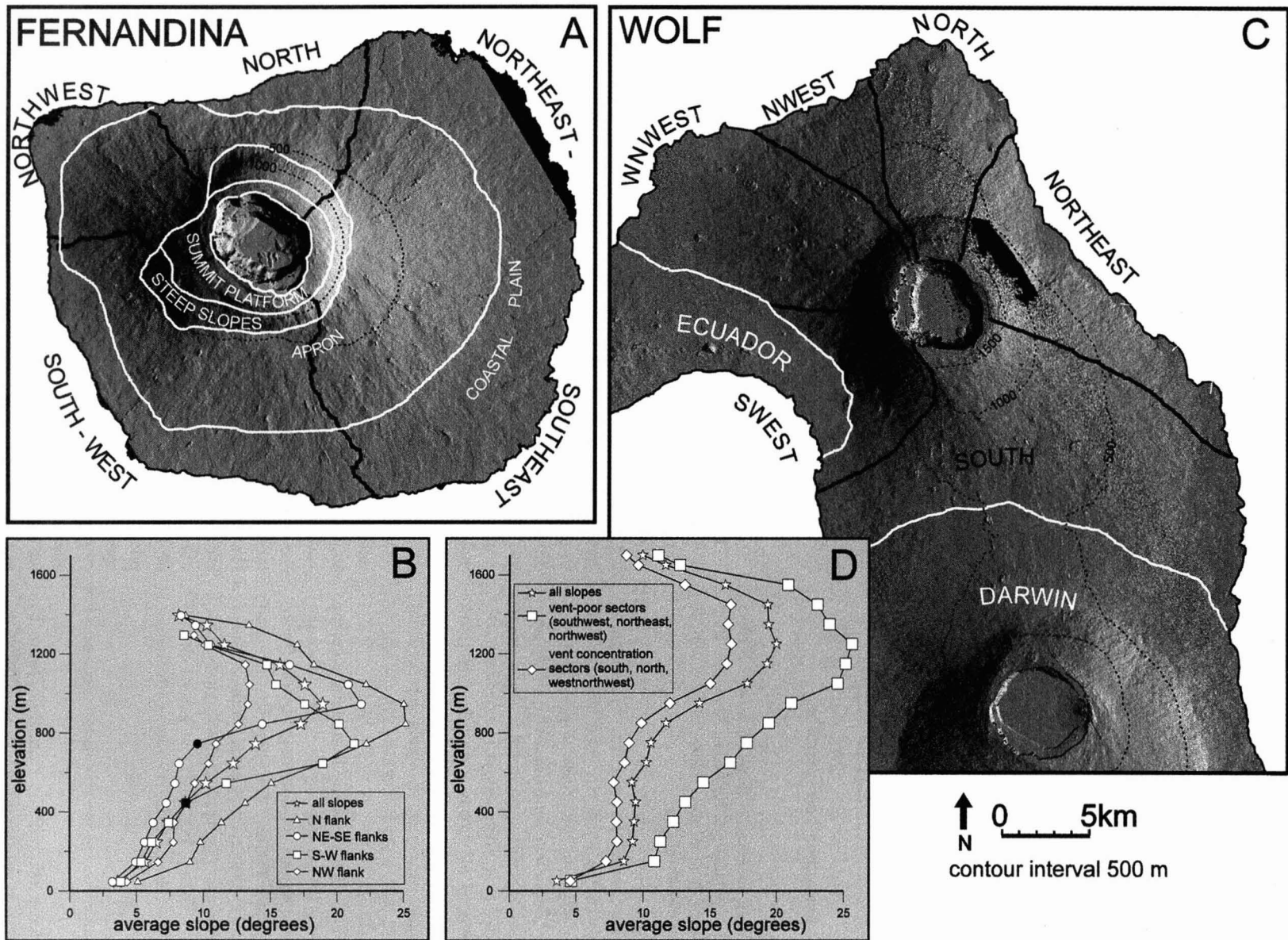


Figure 6. Shaded relief images (a and c) and slope data (b and d) for Fernandina and Wolf, respectively. In (a), heavy white lines and white labels indicate slope regions, and heavy black lines (with labels offshore) indicate flank sectors defined by vent distributions, lava flow ages, and slope characteristics [Rowland, 1996]. Black areas along coast were either outside of the TOPSAR swaths (those with straight inland margins), or were indistinguishable in the radar data from ocean (those with irregular inland margins). In (b), filled symbols indicate uppermost data point on the apron for the northeast-southeast and south-west flank sectors. In (c), heavy black lines (with labels offshore) indicate flank sectors defined by vent distributions mapped from Chadwick and Howard [1991]. Lava deltas are indicated by Id, black areas on northeast flank and southern caldera wall are regions of no data due to radar shadowing.

Table 3. Fernandina Slope Characteristics [from Rowland, 1996]
(A) Slope Regions

Slope Region	Average Slope (°)	Areal Percent (%)	Vent Concentration (vents/km ²)
Coastal Plain	2	40	0.1
Apron	7	47	0.7
Steep Slopes	20	6	1
Summit Platform	10	5	4.7

Table 3. Fernandina Slope Characteristics [from Rowland, 1996]
(B) Flank Sectors

Sector	Elevation Interval (m)	Slope Range (°)	Change in Slope (°/100 m)
N Flank	0-800	5-25	+2.7
	800-900	25	0
	900-1400	25-8	-3.4
NE-SE Flanks	0-700	3-9	+0.9
	700-900	9-22	+6.5
	900-1400	22-8	-2.8
S-W Flanks	0-400	4-8	+1
	400-700	8-22	+4.7
	700-1300	22-8	-2.3
NW Flank	0-1000	4-13	+0.9
	1000-1300	13-9	-1.3

whole, although they are on average 2-3° steeper at any given elevation. Slope data for the youngest portion of the edifice show the greatest amount of variation because small features comprise larger relative areas. For example, slopes approach 20° at about 1000 m in elevation, but decrease sharply owing to the Plaine des Osmondes, the floor of a small avalanche scar. Above this, slopes steepen again and then decrease at ~1500 m, the floor of the caldera. The cone growing within the caldera comprises the highest elevations of the youngest part of the volcano, producing slopes near 20°, and is topped by the Cratere Dolmieu with a floor at ~2400 m.

In general, there are gradual slopes within enclosed craters (e.g., Cratere Dolmieu) and wherever lavas have ponded against an older edifice or avalanche scarp. The steepest slopes on the youngest volcano occur at around 1000 m on the east flank corresponding to fault scarps mapped by Labazuy [1996]. Overall, the flank slopes of

Piton de la Fournaise are the steepest of any of the volcanoes in the present study, even when avalanche scars and valleys are excluded.

SLOPE-FORMING PROCESSES

The morphology of a volcano is a time-integrated record of its eruptive and erosional activity, with various constructive and destructive processes producing characteristic slopes (Table 5). Gradual slopes occur where lava ponds in closed depressions such as calderas. Two volcanoes growing close to each other intersect to form a saddle. Lavas encountering these saddles stagnate and pool, producing large areas of near-horizontal slopes.

Near-horizontal coastal plains occur on most of the examples presented here. These correspond to regions of coalesced lava deltas [Jones and Nelson, 1970; Moore et

Table 4. Slope Statistics for Volcanoes on Isabela, Western Galapagos
(A) Slope Regions on Individual Volcanoes

Slope Region	Average Slope (°)	Areal Percent (%)	Area (km ²)	No. Vents/km ²
Cerro Azul:				
coastal plain, saddle	4.8	41	234	0.1
apron	9.1	40	245	0.6
steep slopes	16.9	13	81	0.6
summit platform	10.5	2	14	2.4
Sierra Negra:				
coastal plain, saddles	4.7	70	1368	0.02
apron	6.3	23	443	0.2
steep slopes	9.9	3	53	0.6
summit platform	8.7	1	29	1.6
Alcedo:				
coastal plain, saddles	5.0	27	193	0.03
apron	7.3	62	436	0.2
steep slopes	18.8	3	26	0.7
summit platform	6.7	1	10	0.3
Darwin:				
coastal plain, saddles	4.7	35	108	0.4
apron	7.7	44	348	0.2
steep slopes	14.8	13	124	0.2
summit platform	9.1	1	15	1.4
Wolf:				
coastal plain and saddle	5.4	15	113	0.1
apron	8.9	66	333	0.5
steep slopes	21.5	11	76	0.4
summit platform	10.8	2	11	1.2
Ecuador:				
rift zone ¹	5.8	80	122	0.6
main: steep slopes (erosional) ¹	36.1	4	0	0
main: summit platform	19.8	4	6	0.2
main: total	17.9	20	31	1.2

¹[Rowland *et al.*, 1994]

Table 4. Slope Statistics for Volcanoes on Isabela, Western Galapagos
(B) Summary of Western Galapagos Slope Regions (Excluding Ecuador)

Slope Region	Average Slope (°)	Average % Area of Volcano	Average No. vents/km ²
coastal plains	4.9	40	0.13
aprons	8.2	45	0.34
steep slopes	16.9	8	0.5
summit platforms	9.1	1	1.4

GRAND COMORO SLOPES

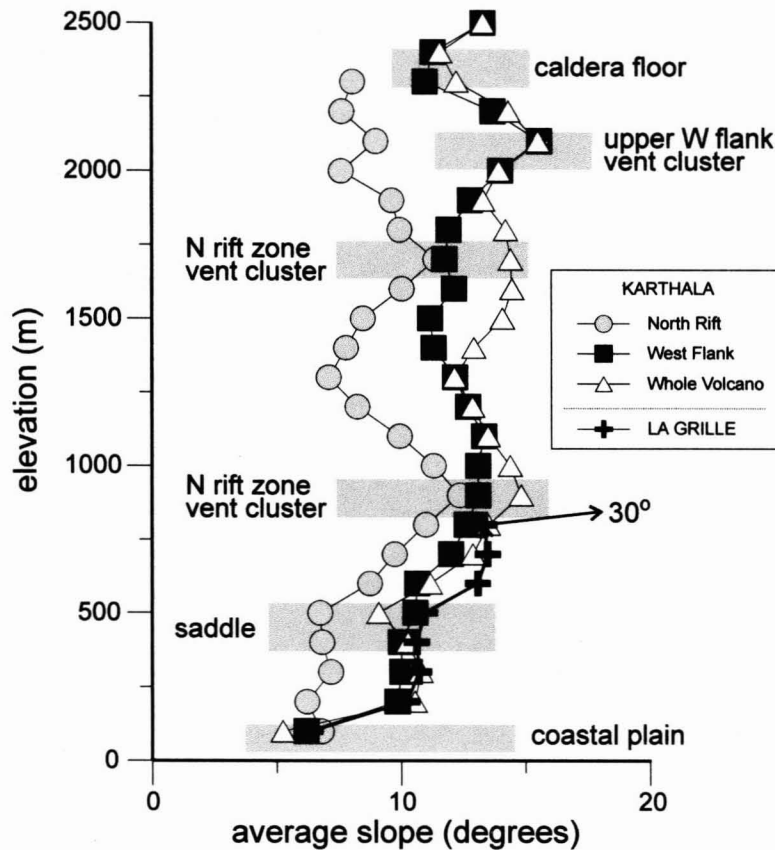


Figure 7. Average slope vs. elevation for Karthala and LaGrille volcanoes, Grand Comoro. Gray boxes highlight particular geologic features that produce distinct slope effects.

al., 1973]. When a lava flow encounters the ocean it shatters as a result of rapid quenching and wave action. Lava builds out across this layer of hyaloclastite to repeat the process farther beyond the pre-eruption shoreline (Figure 9). Because the hyaloclastite/lava interface always occurs at mean sea level, the construction of a lava delta extends the subaerial margin of a volcano outward at a constant elevation, producing near-horizontal coastal slopes.

Lipman and Moore [1996] consider rising relative sea level to be a prerequisite for large coastal plains, but gradual offshore slopes will also enhance their formation. Examples include the nearly 10 km-wide northeast-southeast coastal plain of Fernandina with the shallow Strait of Bolivar immediately offshore, and the northeastern-most subaerial portion of Mauna Loa where an extension of

Mauna Kea occurs offshore [Mark and Moore, 1987; Lipman and Moore, 1996]. Although narrower, coastal plains on the south flank of Kilauea and southwest flank of Mauna Loa have developed despite offshore slopes of 14° or more [Mark and Moore, 1987; Moore and Chadwick, 1995] and subsidence rates of as much as 3 mm/yr [Apple and Macdonald, 1966; Moore and Fornari, 1984; Moore, 1987; Lipman and Moore, 1996]. Within the volcano data set presented here, the widest coastal plains steepen gradually inland. Narrower coastal plains are in some cases bounded on their inland side by steep fault scarps, but elsewhere narrow coastal plains have sharp inland boundaries against steeper slopes that are not fault-generated.

Gradual flank slopes are produced where basalt lava (with a low viscosity and yield strength) comprises a high

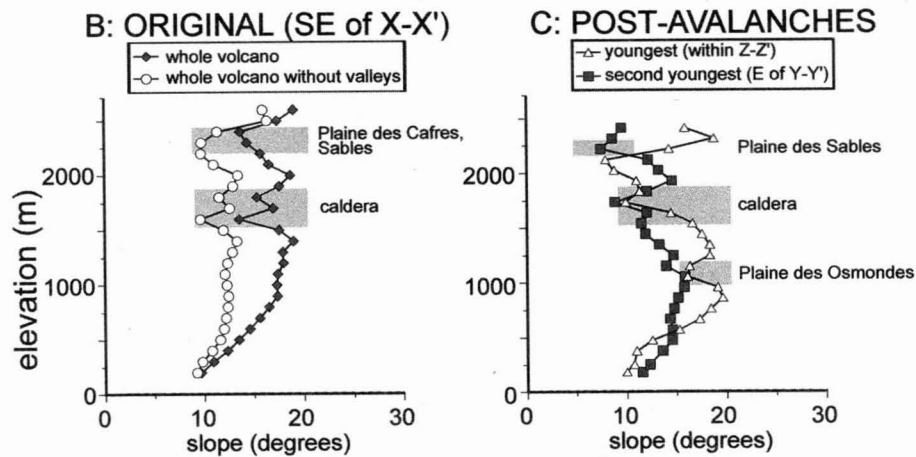
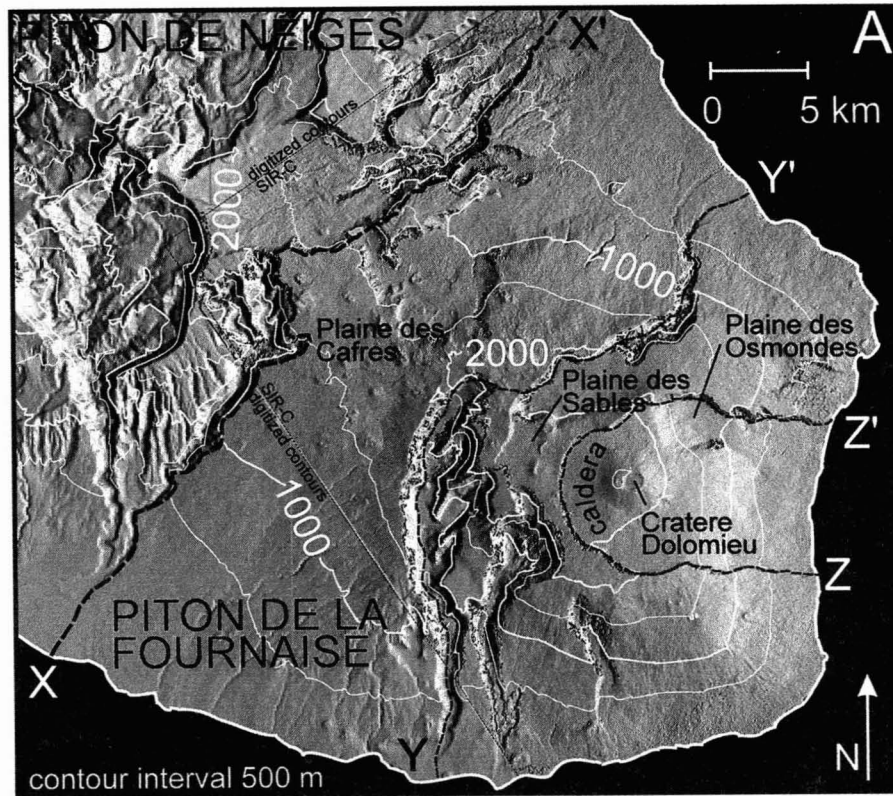


Figure 8. Shaded relief image (a) and graphs of average slope vs. elevation (b and c) for portions of Piton de la Fournaise. Dashed black lines in (a) divide the volcano into sections separated by erosion-modified giant avalanche scars. The scarp corresponding to X-X' separates Piton de la Fournaise from Piton de Neiges. Lines Y-Y' and Z-Z' are avalanche scars wholly within Piton de la Fournaise. Fine dashed line indicates data boundary between interferometrically derived SIR-C and digitized contour-derived DEMs (the SIR-C data did not cover the entire volcano). These contour-derived DEM data were also used to fill radar shadows in the steep erosional valleys although isolated data gaps (black dots) remain. Figure (b) plots average slope versus elevation for all of Piton de la Fournaise with and without inclusion of erosion-modified scarps. Figure (c) plots average slope versus elevation for the portions of the volcano that have built after catastrophic avalanches (with obvious erosional valleys excluded from the analyses). In both graphs, gray boxes highlight particular geologic features that produce distinct slope effects.

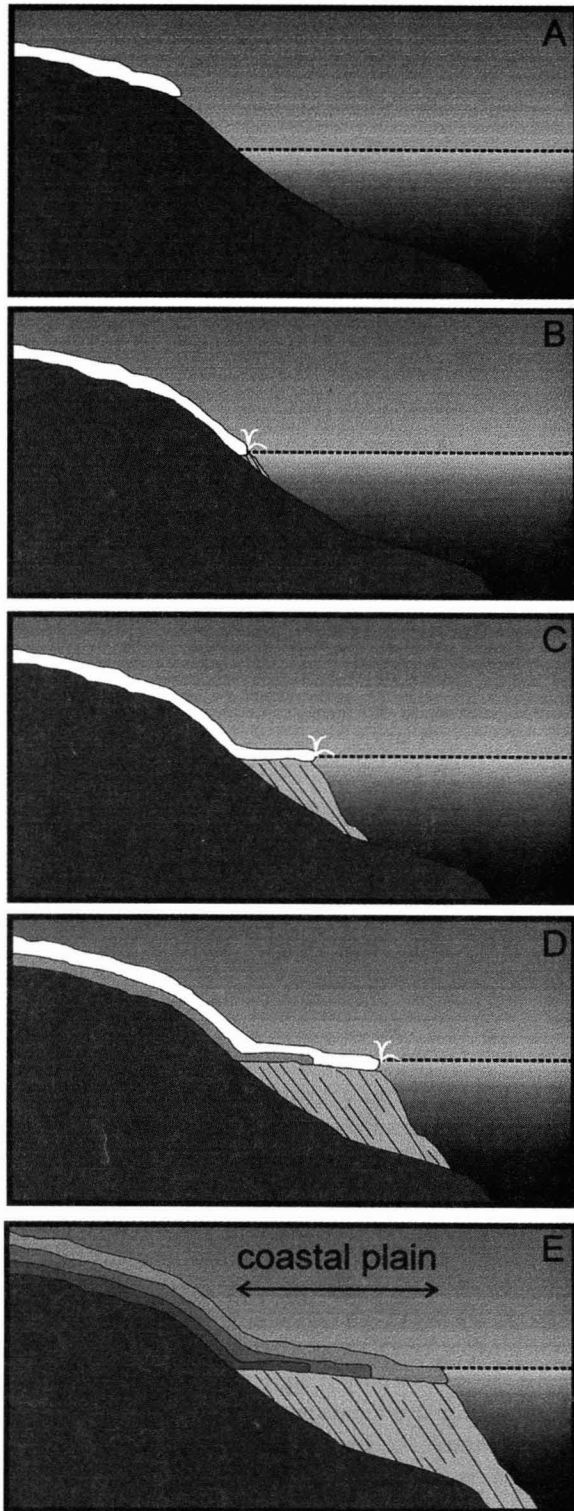


Figure 9. Sequential diagrams (top to bottom) illustrating the construction of a coastal plain at a constant elevation from the coalescence of multiple lava deltas.

percentage of the material and there are no pre-existing steep slopes. Examples include the lower elevations of the western Galapagos volcanoes and the lower 60% of Hawaiian volcanoes. Pyroclastic vents possess slopes that range between 30 and 90° depending on the degree of agglutination of the pyroclasts. As the concentration of vents increases, the contribution from this steeper material causes slopes averaged over a few square kilometers to increase (Figure 10, Table 5).

The highest concentrations of vents occur on the summit platforms of the Galapagos volcanoes and along the rift zones of Mauna Loa, Kilauea, Hualalai, and Karthala. All of these zones of highest vent concentration have average slopes between 5° and 10° and Galapagos data show that in areas with concentrations greater than 1 vent/km² average slope does not increase beyond 11° (Figure 10); the slope contribution from the steep flanks of the vents is moderated by their small relative area and by the fact that they provide barriers behind which lava and tephra can pond. The floors of rift-parallel graben also decrease average rift zone slopes and provide topography within which lavas can pond, such as at Kilauea and Kohala.

Gradual and catastrophic destructive processes produce steep slopes. Fluvial erosion is an example of the former, and examples are obvious on Kohala and Piton de la Fournaise. On both volcanoes the locations of major erosional valleys are controlled by pre-existing faults [Stearns and Macdonald, 1946; Duffield *et al.*, 1982]. Marine erosion was proposed to have formed the steep slopes on Ecuador volcano [Rowland *et al.*, 1994]. Small-scale catastrophic events [e.g., Chadwick *et al.*, 1991] produce and maintain steep caldera walls. Large-scale catastrophic avalanches [e.g., Moore, 1964; Duffield *et al.*, 1982; Moore *et al.*, 1989] produce obvious concave-oceanward scarps on volcanic flanks.

A fourth type of steep slope occurs between regions of rapid and slow vertical growth and can thus be considered constructional in origin. A typical basaltic eruption produces one or more cinder or spatter cones plus a lava flow or flow field. The vent constructs usually comprise <5% of the total area of new material, however, they are often ten times as tall as their associated flows are thick (Figure 11a). Integrating over thousands of eruptions will cause the parts of a volcano where vents are concentrated to grow upward at a rate greater than that of adjacent areas composed mostly of lava. The result is that the part of the volcano connecting these two regions acquires a steep (constructional) slope (Figure 11b and c); the sharper the boundary of the vent concentration zone, the steeper these slopes will be. If the vent concentration zones are also associated with shorter lava flows that do not flow far enough

240 SLOPES OF OCEANIC BASALT VOLCANOES

Table 5. Slope-Forming Processes

Slope-forming Process or Feature	Resultant Slopes	Examples in Present Study
lavas ponded in calderas	near-horizontal (0-5°)	all that have calderas
lavas ponded in saddles	near-horizontal to gradual (0-5°)	all saddles
coastal plains:		Fernandina, Sierra Negra, NE, NW, SW Mauna Loa, NE Kīlauea, Hualalai, NW Karthala
wide, steepening gradually	gradual (2-5°)	
narrow, fault-bounded	gradual (2-5°)	S Kīlauea, W Mauna Loa, W Cerro Azul, E Karthala, NE Wolf
narrow, non fault-bounded	gradual (2-5°)	N Wolf, W Darwin, S Cerro Azul, Karthala (locally), LaGrille (locally)
intermixed vents and lavas	moderate (5-11°)	all Galapagos aprons, all Galapagos summit platforms, rift zone axes of Mauna Loa, Hualalai, Karthala
differential vertical growth	steep (15-40°)	N, S Fernandina, E Wolf, NE, SW Darwin, N Sierra Negra, Cerro Azul, Hualalai, Mauna Loa, Karthala, Piton de la Fournaise
catastrophic flank avalanches	steep (20-50°)	E, W, S Mauna Loa ¹ , S Kīlauea ² , E Karthala ³ , Piton de la Fournaise ⁴ , W Ecuador ^{5,6} , SW Cerro Azul ⁷
caldera collapses and avalanches	steep (30-90°)	all calderas in study
fluvial (fault-controlled) erosion	steep (20-50°)	Kohala, Piton de la Fournaise
marine erosion	steep (20-40°)	Ecuador ⁸
glacial moraines	steep (20-40°)	Mauna Kea, Mauna Loa (?)

¹Moore *et al.*, [1989], ²Dvorak *et al.*, [1986], ³Bachèlery and Coudray, [1993], ⁴Duffield *et al.*, [1982], ⁵Simkin, [1984], ⁶Chadwick and Howard, [1991], ⁷Nauman and Geist, [1999], ⁸Rowland *et al.*, [1994]

to reach the lowest flanks, this growth contrast will be enhanced [Simkin, 1972; Nauman and Geist, 1999].

In an idealized case of arcuate vents concentrated around a caldera (Figure 11d), steep, convex-outward slopes develop. The clearest example of this process is on Fernandina where arcuate vent concentrations in the summit platform average ~5 vents/km² and are situated less than 1-2 km in plan view from the nearby apron having only ~1 vent/km². At Fernandina the concentration of arcuate vents is higher on the north and south portions of the summit platform whereas the north and south aprons have the fewest radial vents. Thus the best-developed steep slopes on the volcano correspond to the highest contrast in vertical growth rate between apron and summit platform. The high number of radial vents in the northeast to southeast Fernandina apron [Chadwick and Howard, 1991;

Rowland, 1996] produces less of a vent-concentration contrast between the summit platform and apron, and here the steep slopes are poorly developed. Essentially no change in vent concentration occurs all the way up the northwest flank and steep slopes have not developed there.

Mouginis-Mark *et al.* [1996] noted that steep flank slopes on the western Galapagos volcanoes did not correlate consistently with high concentrations of arcuate vents. Given the relationship for Fernandina outlined above, steep Galapagos slopes not only require a high concentration of arcuate vents, but also a paucity of radial vents in the adjacent apron. Figure 12b maps the highest concentrations of arcuate vents on the summit platform, concentrations of radial vents on the apron, and steep slopes. In addition to the case at Fernandina described above, the east sector of Wolf, northeast and southwest sectors of Darwin, and the

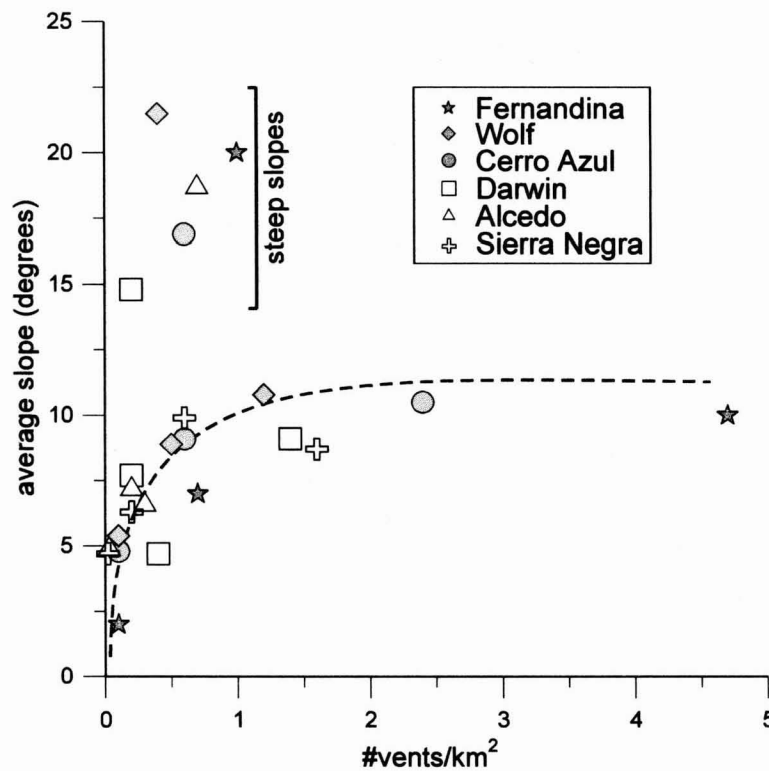


Figure 10. Graph of average slope versus number of vents per unit area for the slope sections of the six western Galapagos volcanoes. Data for the coastal plains, aprons, and summit platforms form a somewhat asymptotic trend of increasing slope with increasing vent concentration (generalized by the dashed line). Steep slope sections fall distinctly off this trend.

north sector of Sierra Negra illustrate a correlation between a high concentration of arcuate vents on the summit platform, low concentration of radial vents on the adjacent apron, and steep slopes. The opposite situation (concentrations of radial vents and lack of steep slopes) can be found at northwest Fernandina, east Sierra Negra, and southeast Darwin. Note that some steep slopes do occur where there are concentrations of radial vents such as northeast-southeast Fernandina, southeast Wolf, north and south Alcedo, and most of Cerro Azul, but that in all but the Cerro Azul example these steep slopes are relatively minor.

Although not as distinct, a similar relationship occurs where the vent concentrations are linear rift zones, such as on Mauna Loa, Hualalai, and Karthala (Figures 12a, c). The axes of these linear rift zones grow upward faster than the lower elevations (where lavas accumulate), with the result that the flanks of the rift zones become the steepest parts of the volcanoes (ignoring mass-wasting features;

Figure 11e). The axes of the rift zones themselves have relatively gradual slopes so that particularly for Mauna Loa and Hualalai, they stand out distinctly in slope images.

Rift zones oriented northwest, southwest, and southeast occur on Piton de la Fournaise [Duffield *et al.*, 1982]. The northeast and southwest coastal regions (comprised almost wholly of lava) have gradual slopes, as does the northwest rift zone axis, and the slopes between these coasts and the axis are steeper (Figure 12d). The northeast and southwest rift zones are bounded by numerous erosional valleys, precluding a similar slope assessment.

DISCUSSION

The volcanoes studied here contain different combinations of slope features, and these have combined spatially and temporally to produce a variety of volcano morphologies. Except for catastrophic avalanche and caldera scarps,

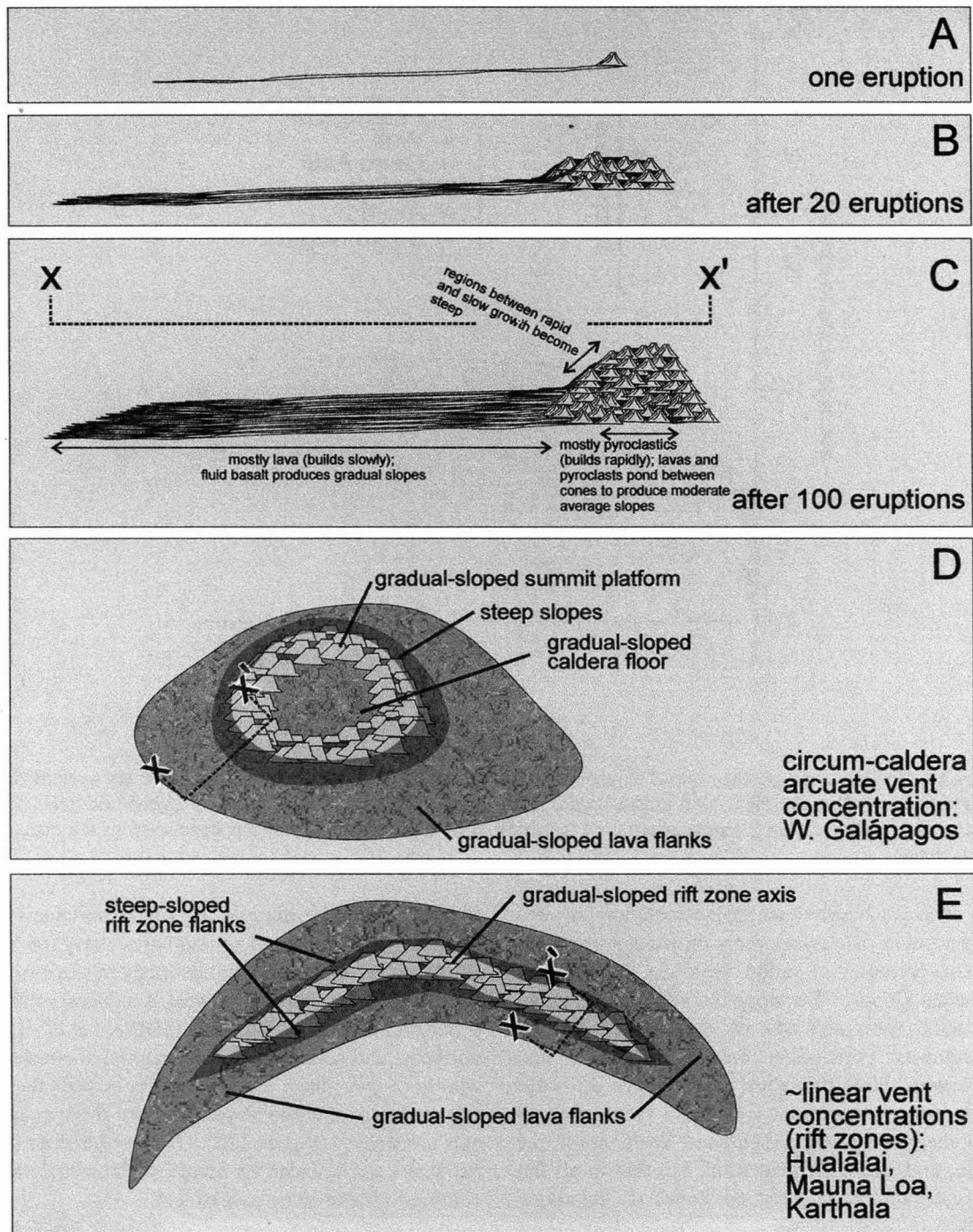


Figure 11. Diagrams (without vertical exaggeration) illustrating the development of constructional steep slopes. (a) a single eruption produces a pyroclastic vent of small areal extent but relatively large height compared to the associated lava flow. (b) the situation after 20 eruptions, assuming that eruptive vents are concentrated into a small portion of the volcano (e.g., a rift zone or arcuate vent zone). (c) the situation after 100 eruptions. Note that the steepest slopes correspond to the flanks of the vent-concentration zones. (d) cartoon of a volcano where the vent concentration zone forms an annulus around a caldera such as in the western Galapagos. (e) cartoon of a volcano where the vent concentration zone is more or less linear such as the rift zones of Hawaiian volcanoes and Karthala.

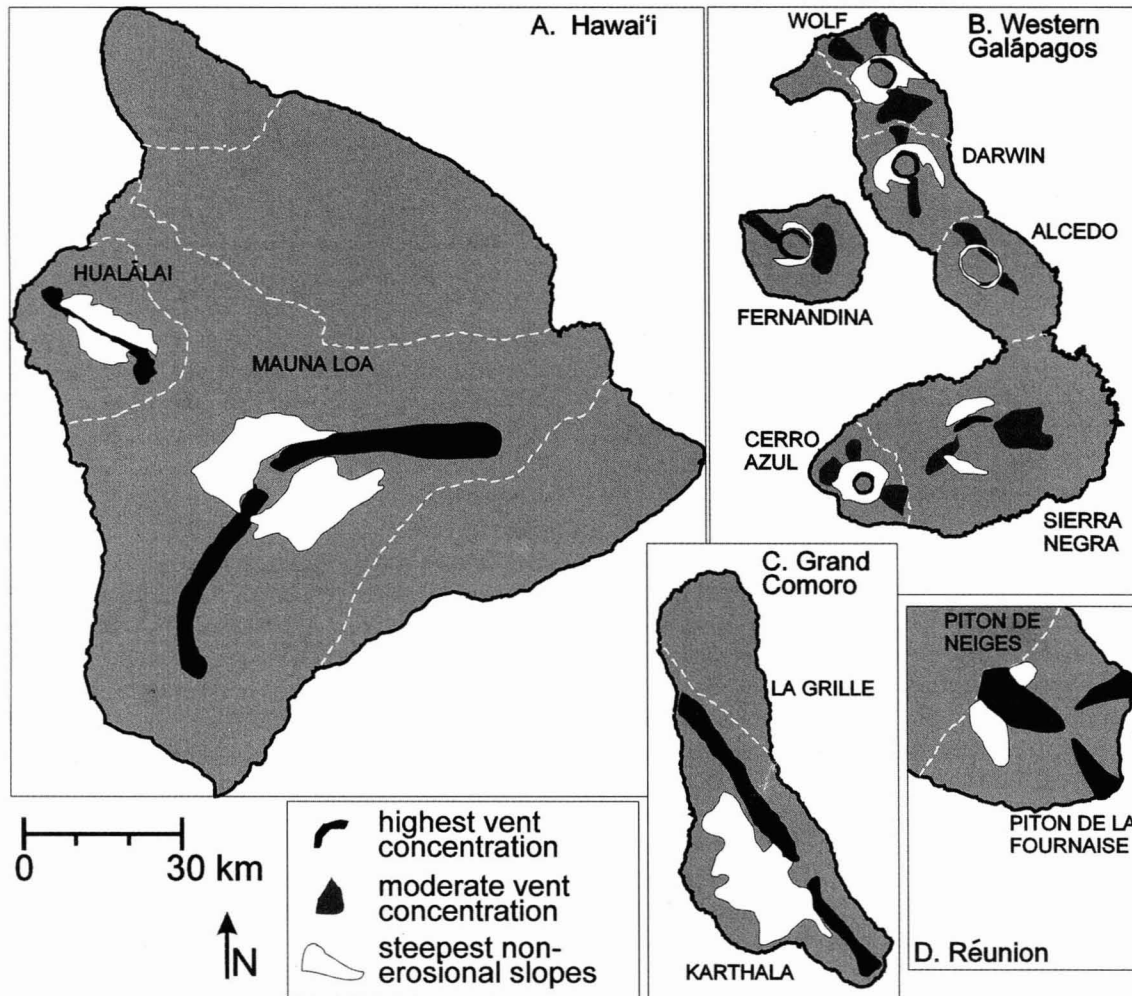


Figure 12. Maps showing vent-concentration zones and associated slope features for the volcanoes discussed in the text. For Hawaii (a), note that the steepest slopes of Mauna Loa and Hualalai (not counting avalanche and fault scarps) occur on the flanks of the well-defined rift zones. In the western Galapagos (b), note that steep slopes occur at all locations where there is a combination of high arcuate vent concentrations with no radial vent concentration. On Karthala (c), the situation is similar to that in Hawaii, although the data bias (see text) and large amount of collapse features on the east flank [Bachèlery and Coudray, 1993] allow only one rift zone flank (the west) to be included in the analysis. On Piton de la Fournaise (d) only the flanks of the northwest rift zone can be assessed because of the proximity of erosional and faulted slopes to the other two rift zones.

these slope features (whether steep or gradual) are the integrated result of many events and therefore reflect long-term behavior. Thus they are good indicators of the types and distribution of activity on each volcano. Additionally, if one slope type can be shown to be forming at the expense of another, a change in activity can be inferred. It is important to note that a combination of processes is required to account for the morphology of each volcano.

As summarized by Moore and Mark [1992], the combined effects of summit vent concentrations [Peterson and

Moore, 1987] and cooler lavas during the post-shield alkalic stage of a Hawaiian volcano produce an upward steepening of the central part of these volcanoes (Hualalai, Mauna Kea, and Kohala; Figure 2b). A similar relationship can be cited for La Grille [Bachèlery and Coudray, 1993].

Simkin [1972] considered the Galapagos summit platforms to be a product of the interplay between caldera subsidence and infilling, and although not as distinctly as those with summit platforms, all the other volcanoes in this study

with calderas also become less steep at their highest elevations. The data of Walker [1988] and Delaney *et al.*, [1998] indicate that at Kīlauea downward sagging affects not only the caldera floor but the entire summit region as well. Lava accumulation combined with this broad-scale sagging produces a volcano with gradually sloping upper elevations.

Average unfaulted slopes of Kīlauea are extremely gradual through the entire elevation range. Approximately 50% of the surface is lavas ponded against the flank of Mauna Loa [Holcomb, 1987]. Additionally, the Kīlauea rift zones are regions of subsidence, in part because the south flank of Kīlauea moves southward so readily [e.g., Dvorak *et al.*, 1986]. The result is minimal topographic contrast between the rift zone axes and the lavas ponded against Mauna Loa and overall low average slopes.

The steepest slopes of Mauna Kea reflect the locations of end moraines produced during Pleistocene glaciation [Moore and Mark, 1992]. A less-distinct steepening of Mauna Loa centered on the 80% elevation level has been attributed to short caldera overflows [Moore and Mark, 1992; Lipman, 1995] or inflation [Lipman, 1995]. An alternative hypothesis, unsupported by data, is that moraines also formed on Mauna Loa but have been buried by lava.

It has been proposed that the western Galapagos calderas have been both shallow and deep throughout their history [Chadwick and Howard, 1991; Munro and Rowland, 1996] and that their present depths do not necessarily represent inherent volcano differences or positions within an evolutionary sequence. However, flank morphology corresponds to caldera depth [Mouginis-Mark *et al.*, 1996] and is less likely to vary over short periods of time, suggesting that there are indeed inherent differences between the two groups of Galapagos volcanoes [see also Nordlie, 1973]. Probably all 6 western Galapagos calderas have filled and collapsed numerous times, but those of Sierra Negra, Darwin, and Alcedo have spent more time infilled whereas those of Fernandina, Cerro Azul, and Wolf have spent more time collapsed. For these latter three the time-averaged state of the caldera has been deep with high, unbuttressed walls, so there has been more time with stress conditions favorable for arcuate vents [McGuire and Pullen, 1989; Rowland, 1996], faster growth of the central part of the volcano, and better developed constructional steep flanks.

In Hawaii, some volcano boundaries correspond to distinct changes in slope as well as contrasts in recent eruptive activity (e.g., Mauna Kea and Kohala). On the other hand, there is no distinct slope boundary between Hualalai and Mauna Loa even though Hualalai has erupted ~200 times in the past 10,000 years [Moore *et al.*, 1987] while Mauna

Loa has erupted ~360 times in only the past 4000 years [Lockwood and Lipman, 1987]. This may be because a relatively high-productivity part of Hualalai (the southeast rift zone) is juxtaposed against a low-productivity part of Mauna Loa (the west flank).

Little is known about relative activities of the western Galapagos shields. Based on the Hawaiian analogy, distinct slope boundaries (Plate 1) indicate that the east rift zone of Ecuador has been more active than the west flank of Wolf, that Darwin is more active than Alcedo, and that Sierra Negra is more active than Cerro Azul. However, Nauman and Geist [1999] note that lavas from Sierra Negra and Cerro Azul interfinger equally at their current boundary. In recent times the two have apparently been equally active but the slope data suggest that the time averaged activity of Sierra Negra has been greater than that of Cerro Azul.

A distinct surface boundary occurs between the vegetated south flank of Wolf and the unvegetated north flank of Darwin [Benchley and Franklin, 1999], but there is no corresponding distinct change in slope (Plate 1b). We consider the slope data to reflect a longer-term integration of the (relatively equal) activity of these two volcanoes. There is no distinct change in slope corresponding to the surface boundary of rhyolite ash on Alcedo that may be more than 100 Ka in age [Geist *et al.*, 1994] and flows of the north flank of Sierra Negra that are ≤ 1 Ka [Reynolds *et al.*, 1995]. The two volcanoes are separated by Istmo Perry, which with an average elevation of < 20 m and a width of ~11 km, likely formed recently as Sierra Negra grew northward; it represents a merging of two coastal plains and no distinct change in slope would be expected.

Another example occurs on Grand Comoro where the change in slope between Karthala and LaGrille (Plate 1c) does not correspond exactly to the surface-unit-derived volcano boundary of Bachèlery and Coudray [1993], which has more of an east-west orientation. The surface units give the distribution of only the most recent activity whereas slope data suggest that structurally Karthala extends farther to the northwest and LaGrille extends farther to the southeast. DePaolo and Stolper [1996] derived saddle-migration equations for cases where two volcanoes grow at different relative rates, and the application of these to the Galapagos and Grand Comoro examples may provide quantitative information on their relative growth rates.

The relationships between lava deltas (or coastal plains composed of coalesced lava deltas) and the slopes immediately inland provide information about long-term volcano subsidence. Specifically, coastal plains that are broad and steepen gradually inland indicate that volcanism is able to keep pace with subsidence. Examples are Mauna Loa,

Hualalai, Fernandina, and Sierra Negra. A lack of lava deltas indicates that subsidence dominates, such as on Mauna Kea and Kohala [Moore and Mark, 1992]. An intermediate situation occurs where lava deltas have distinct inland margins against steeper (but not fault-generated) slopes. We suggest that these cases indicate a dominance by subsidence but not to the extent that occasional flows are unable to form localized lava deltas. Examples of these are listed in Table 5.

Lava delta relationships allow us to speculate about subsidence rates where they have not been measured. For example, in the western Galapagos, one endmember explanation is that subsidence is constant under all six volcanoes but that long-term eruption rates at Fernandina and Sierra Negra are higher. The other is that long-term eruption rates are equal but that subsidence is less under Fernandina and Sierra Negra. We prefer the former endmember, and suggest that lower long-term eruption rates at Wolf, Darwin, and Cerro Azul cannot keep pace with subsidence with the result being only localized lava deltas.

On Grand Comoro both Karthala and LaGrille possess lava deltas juxtaposed against steeper, but non-faulted, inland slopes. However, Karthala is clearly the more active of the two [Bachèlery and Coudray, 1993; Simkin and Siebert, 1994]. Unequal eruption rates combined with similar lava delta properties suggest unequal subsidence rates, with Karthala subsiding faster.

Extensive lava deltas are essentially nonexistent on Piton de la Fournaise, even along the east coast where most of the young lavas have entered the ocean, and despite the fact that the volcano is highly active, having erupted more than 150 times since 1640 [Simkin and Siebert, 1994]. This suggests considerable subsidence rates and is supported by the occurrence in a drill hole of subaerially erupted flows as deep as 728 m below present sea level [Rançon *et al.*, 1989].

CONCLUSIONS

We conclude that quantitative slope data are useful for analyzing the contributions of various geological processes to the form of a volcano. Contrasts in slopes indicate juxtapositions of processes (e.g., subsidence vs. lava delta formation) or juxtaposition of different degrees of eruptive activity on neighboring volcanoes. Although the morphologies of all 15 volcanoes studied here can be produced by the same set of processes, the general differences that exist between the geographic groups of volcanoes indicate that there are patterns in the distribution of these processes.

Examples include concentrations of vents around the caldera versus along-rift zones or in radial patterns as well as relative eruptive activity indicated by erosional features and lava delta formation. However, within any one of these geographic groups and even on a single volcano, different spatial and temporal distributions of, and dominance by, various slope-forming processes can be defined. Although this complexity does not preclude modeling of the consequences of volcano morphology (e.g., on gravitational stresses and dike orientations; Chadwick and Dieterich, 1995), it does suggest that forward modeling of single processes [e.g., Cullen *et al.*, 1987] will not reproduce realistic morphologies.

This study illustrates that remote sensing data are as useful for characterizing integrated volcanic histories as they are for studying the current surface or ongoing events. The morphological analyses presented here were of a spatial scale that did not cause any one of the remotely sensed data types to be more or less useful. The interpolated and mosaicking drawbacks of the orthophoto-derived DEMs are essentially balanced by the drawbacks of the interferometric techniques (radar shadows, poor knowledge of baselines). Given that interferometric DEMs will soon be available for most of the Earth from SRTM [Zebker *et al.*, 1994], their utility for morphological volcano studies will certainly increase. Digital topography data are also essential for realistic modeling of volcanic processes, including the emplacement of lava flows and lahars. The topographic data presented here could provide excellent real substrates over which to test the effects of changing model parameters.

The analyses presented here were made without the benefit of field checking (although field work by others provides significant constraints). Thus comparable analyses of time-averaged volcanic processes could also be performed on extraterrestrial volcanoes as long as digital elevation data are available. We therefore note with interest that the MOLA instrument currently collecting topographic profiles of Mars [Smith *et al.*, 1998], will facilitate quantitative morphological investigation of Martian volcanoes.

Acknowledgments. W. Chadwick and J. Fink provided useful, detailed, reviews, and we thank P. Mougini-Mark for also critically reading this manuscript. These data were initially compiled for presentation at a Penrose Conference on Oceanic Volcanism (Galapagos Islands, 1998); SKR thanks the conference organizers (D. Geist, W. Borson, and K. Harp) and the Geological Society of America for their support. This research was funded by NASA grant #NAG 5-3000 from the Digital Topography Program and JPL grant no. 958457 from the SIR-C program, both to P. Mougini-Mark. This is SOEST contribution no. 4841 and HIGP publication no. 1072.

REFERENCES

- Apple, R. A., and G. A. Macdonald, The rise of sea level in contemporary times at Honaunau, Kona, Hawaii, *Pac. Sci.*, 20, 125-136, 1966.
- Bachèlery, P., and J. Coudray, Carte volcano-tectonique de la Grande Comore (Ngazidja), with explanation booklet. République Fédérale Islamique des Comores Centre National de Documentation et de Recherche Scientifique, 1993.
- Benchley, P., and S. Franklin, Galapagos paradise in peril, *National Geographic*, 195, 2-31, 1999.
- Chadwick, W. W., and K. A. Howard, The pattern of circumferential and radial eruptive fissures on the volcanoes of Fernandina and Isabela islands, Galapagos, *Bull. Volcanol.*, 55, 259-275, 1991.
- Chadwick, W. W., T. D. Roy, and A. Carrasco, The September 1988 intracaldera avalanche and eruption at Fernandina volcano, Galapagos Islands, *Bull. Volcanol.*, 55, 276-286, 1991.
- Chadwick, W. W., and J. H. Dieterich, Mechanical modeling of circumferential and radial dike intrusion on Galapagos volcanoes, *J. Volcanol. Geotherm. Res.*, 66, 37-52, 1995.
- Cullen, A., A. R. McBirney, and R. D. Rodgers, Structural controls on the morphology of Galapagos shields, *J. Volcanol. Geotherm. Res.*, 34, 143-151, 1987.
- Delaney, P. T., R. P. Denlinger, M. Lisowski, A. Miklius, P. G. Okubo, A. T. Okamura, and M. K. Sako, Volcanic spreading at Kilauea, 1976-1996, *J. Geophys. Res.*, 103, 18,003-18,023, 1998.
- DePaolo, D. J., and E. M. Stolper, Models of Hawaiian volcano growth and plume structure: Implications of results from the Hawaii Scientific Drilling Project. *J. Geophys. Res.*, 101, 11,643-11,654, 1996.
- Duffield, W. A., L. Stieltjes, and J. Varet, Huge landslide blocks in the growth of Piton De La Fournaise, La Réunion and Kilauea volcano, Hawaii. *J. Volcanol. Geotherm. Res.*, 12, 147-160, 1982.
- Dvorak, J. J., A. T. Okamura, T. T. English, R. Y. Koyanagi, J. S. Nakata, M. K. Sako, W.R. Tanigawa, and K.M. Yamashita, Mechanical response of the south flank of Kilauea volcano, Hawaii, to intrusive events along the rift zones, *Tectonophysics*, 124, 193-209, 1986.
- Evans, D. L., T. G. Farr, H. A. Zebker, J. J. van Zyl, and P. J. Mougini-Mark, Radar interferometry studies of the Earth's topography, *EOS Trans. AGU*, 73, 553-558, 1992.
- Farr, T., D. Evans, H. Zebker, D. Harding, J. Bufton, T. Dixon, S. Vetrella, and D. Gesch, Mission in the works promises precise global topographic data, *EOS Trans. AGU*, 76, 225-229, 1995.
- Geist, D., K. A. Howard, A. M. Jellinek, and S. Rayder, Volcanic history of Volcán Alcedo, Galapagos Archipelago: A case study of rhyolitic oceanic volcanism, *Bull. Volcanol.*, 56, 243-260, 1994.
- Holcomb, R. T., Eruptive history and long term behavior of Kilauea Volcano, in *Volcanism in Hawaii*, U.S. Geol. Surv. Prof. Pap. 1350, edited by R. W. Decker, T. L. Wright, and P. H. Stauffer, pp. 261-350, 1987.
- Imhoff, M., M. Story, C. Vermillion, F. Khan, and F. Polcyn, Forest canopy characterization and vegetation penetration assessment with space-borne radar, *IEEE, GE-24*, 535-542, 1986.
- Izenberg, N. R., R. E. Arvidson, R. A. Brackett, S. S. Sastchi, G. R. Osburn, and J. Dohrenwend, Erosional and depositional patterns associated with the 1993 Missouri River floods inferred from SIR-C and TOPSAR radar data, *J. Geophys. Res.*, 101, 23,194-23,167, 1996.
- Jones, J. G., and P. H. H. Nelson, The flow of basalt lava from air into water—Its structural expression and stratigraphic significance, *Geol. Mag.*, 107, 13-19, 1970.
- Labazuy, P., Recurrent landslides events on the submarine flank of Piton de la Fournaise Volcano (Reunion Island), in *Volcano Instability on the Earth and Other Planets*, edited by W. J. McGuire, A. P. Jones, and J. Neuberger, *Geol. Soc. Spec. Pub.* 110, 295-306, 1996.
- Lang, H. R., and R. Welch, Algorithm theoretical basis document for ASTER digital elevation models (Standard Product AST14), *Algorithm Theoretical Basis Document AST-09*, web address: <http://asterweb.jpl.nasa.gov/asterhome/atbd/docs.htm>, 1996.
- Lipman, P. W., Declining growth of Mauna Loa during the last 100,000 years: Rates of lava accumulation vs. gravitational subsidence, in *Mauna Loa Revealed: Structure, Composition, History, and Hazards*, *Geophys. Monogr. Ser.*, vol. 92, edited by J. M. Rhodes and J. P. Lockwood, pp. 45-82, AGU, Washington, D.C., 1995.
- Lipman, P. W., and J. G. Moore, Mauna Loa lava accumulation rates at the Hilo drill site: Formation of lava deltas during a period of declining overall volcanic growth, *J. Geophys. Res.*, 101, 11,631-11,641, 1996.
- Lockwood, J. P., and P. W. Lipman, Holocene eruptive history of Mauna Loa Volcano, in *Volcanism in Hawaii*, U.S. Geol. Surv. Prof. Pap. 1350, edited by R. W. Decker, T. L. Wright, and P. H. Stauffer, pp. 509-536, 1987.
- Mark, R. K., and J. G. Moore, Slopes of the Hawaiian Ridge, in *Volcanism in Hawaii*, U.S. Geol. Surv. Prof. Pap. 1350, edited by R. W. Decker, T. L. Wright, and P. H. Stauffer, pp. 101-107, 1987.
- McBirney, A. R., and H. Williams, Geology and petrology of the Galapagos Islands, *Mem. Geol. Soc. Am.*, 118, 197 pp., 1969.
- McGuire, W. J., and A. D. Pullen, Location and orientation of eruptive fissures and feeder-dykes at Mount Etna: Influence of gravitational and regional tectonic stress regimes, *J. Volcanol. Geotherm. Res.*, 38, 235-344, 1989.
- Moore, J. G., Giant submarine landslides on the Hawaiian ridge, *U.S. Geol. Surv. Prof. Pap.*, 501-D, 95-98, 1964.
- Moore, J. G. Subsidence of the Hawaiian Ridge, in *Volcanism in Hawaii*, U.S. Geol. Surv. Prof. Pap. 1350, edited by R. W. Decker, T. L. Wright, and P. H. Stauffer, pp. 85-100, 1987.
- Moore, J. G., and W. W. Chadwick, Jr., Offshore Geology of Mauna Loa and Adjacent Areas, Hawaii, in *Mauna Loa Revealed: Structure, Composition, History, and Hazards*, *Geophys. Monogr. Ser.*, vol. 92, edited by J. M. Rhodes and J. P. Lockwood, pp. 21-44, AGU, Washington, D.C., 1995.
- Moore, J. G., and D. A. Clague, Volcano growth and evolution of

- the island of Hawaii, *Geol. Soc. Am. Bull.*, 104, 1471-1484, 1992.
- Moore, J. G., and D. J. Fornari, Drowned reefs as indicators of the rate of subsidence of the Island of Hawaii, *J. Geology*, 92, 752-759, 1984.
- Moore, J. G. and M. K. Mark, Morphology of the Island of Hawaii, *GSA Today*, 2, 257-262, 1992.
- Moore, J. G., R. L. Phillips, R. W. Grigg, D. W. Peterson, and D. A. Swanson, Flow of lava into the sea, 1969-1971, Kilauea Volcano, Hawaii, *Bull. Geol. Soc. Am.* 84, 537-546, 1973.
- Moore, J. G., D. A. Clague, R. T. Holcomb, P. W. Lipman, W. R. Normark, and M. E. Torresan, Prodigious submarine landslides on the Hawaiian ridge. *J. Geophys. Res.*, 94, 17,465-17,484, 1989.
- Moore R. B., D. A. Clague, M. Rubin, and W. A. Bohrsen, Hualalai Volcano: A preliminary summary of geologic, petrologic, and geophysical data, in *Volcanism in Hawaii, U.S. Geol. Surv. Prof. Pap. 1350*, edited by R. W. Decker, T. L. Wright, and P. H. Stauffer, pp. 571-585, 1987.
- Mouginis-Mark, P. J., Preliminary observations of volcanoes with the SIR-C radar, *IEEE*, 33, 934-941, 1995.
- Mouginis-Mark, P. J., S. K. Rowland, and H. Garbeil, Slopes of western Galapagos volcanoes from airborne interferometric radar. *Geophys. Res. Lett.*, 23, 3767-3770, 1996.
- Munro, D. C., and S. K. Rowland, Caldera morphology in the western Galapagos and implications for volcano eruptive behavior and mechanisms of caldera formation, *J. Volcanol. Geotherm. Res.*, 72, 1996.
- Nauman T., and D. Geist, Physical volcanology and structural development of Cerro Azul Volcano, Isabela Island, Galapagos: Implications for the development of Galapagos-type shield volcanoes, *Bull. Volcanol.*, in press, 1999.
- Nordlie, B. E., Morphology and structure of the western Galapagos volcanoes and a model for their origin, *Geol. Soc. Am. Bull.*, 84, 2931-2956, 1973.
- Panton, D. J., A flexible approach to digital stereo mapping: *Photogram. Eng. Rem. Sens.*, 44, 1499-1512, 1978.
- Peterson D. W., and R. B. Moore, Geologic history and evolution of geologic concepts, Island of Hawaii, in *Volcanism in Hawaii, U.S. Geol. Surv. Prof. Pap. 1350*, edited by R. W. Decker, T. L. Wright, and P. H. Stauffer, pp. 149-189, 1987.
- Rançon, J. P., P. Lerebour, and T. Augé, The Grand Brule exploration drilling: new data on the deep framework of the Piton de la Fournaise Volcano. Part 1: lithostratigraphic units and volcanostructural implications, *J. Volcanol. Geotherm. Res.*, 36, 113-127, 1989.
- Reynolds, R. W., D. Geist, and M. D. Kurz, Physical volcanology and structural development of Sierra Negra volcano, Isabela Island, Galapagos archipelago, *Geol. Soc. Am. Bull.*, 107, 1398-1410, 1995.
- Rowland, S. K., D. C., Munro, and V. Perez-Oviedo, Volcán Ecuador, Galapagos Islands: Erosion as a possible mechanism for the generation of steep-sided basaltic volcanoes, *Bull. Volcanol.*, 56, 271-283, 1994.
- Rowland, S. K., Slopes, lava flow volumes, and vent distributions on Volcán Fernandina, Galapagos Islands, *J. Geophys. Res.*, 101, 27,657-27,672, 1996.
- Rowland, S. K., M. E. MacKay, H. Garbeil, and P. J. Mouginis-Mark, Topographic analyses of Kīlauea Volcano, Hawaii, from interferometric airborne radar, *Bull. Volcanol.*, 61, 1-14, 1999.
- Simkin, T., Origin of some flat-topped volcanoes and guyots, *Mem. Geol. Soc. Am.*, 132, 183-193, 1972.
- Simkin, T., Geology of Galapagos Islands, in *Galapagos (Key Environments)*, edited by R. Parry, pp. 15-41, Pergamon Press, Oxford, 1984.
- Simkin T., and L. Siebert, Volcanoes of the World, 2nd ed., 349 pp., Geoscience, Tucson, Ariz., 1994.
- Smith, D. E., M. T. Zuber, H. V. Frey, J. B. Garvin, J. W. Head, D. O. Muhleman, G. H. Pettengill, R. J. Phillips, S. C. Solomon, H. J. Zwally, W. B. Banerdt, and T. C. Duxbury, Topography of the northern hemisphere of Mars from the Mars Orbiter Laser Altimeter, *Science*, 279, 1686-1692, 1998.
- Stearns, H. T., and G. A. Macdonald, Geology and ground-water resources of the Island of Hawaii, *Hawaii Division of Hydrography Bull.*, 9, 363 pp., 1946.
- USGS, Digital Elevation Models Data Users Guide, 5, 51 pp., 1990.
- Walker, G. P. L., Three Hawaiian calderas: An origin through loading by shallow intrusions? *J. Geophys. Res.*, 93, 14,773-14,784, 1988.
- Welch, R., T. Jordon, H. Lang, and H. Murakami, ASTER as a source of topographic data in the late 1990's, *IEEE Trans. Geosci. Rem. Sens.*, 36, 4, 1282-1289, 1998.
- Williams, H., and A. R. McBirney, *Volcanology*, 397 pp., Freeman, Cooper & Co., San Francisco, 1979.
- Zebker, H. A., and R. Goldstein, Topographic mapping from interferometric SAR observations. *J. Geophys. Res.*, 91, 4993-4999, 1986.
- Zebker, H. A., S. N. Madsen, J. Martin, K. B. Wheeler, T. Miller, Y. Lou, G. Alberti, S. Vetrella, and A. Cucci, The TOPSAR interferometric radar topographic mapping instrument, *IEEE Trans. Geosci. Rem. Sens.*, 30, 933-940, 1992.
- Zebker, H. A., T. G. Farr, R. P. Salazar, and T. Dixon, Mapping the world's topography using radar interferometry: the TOPSAR mission, *IEEE Trans. Geosci. Rem. Sens.*, 82, 1744-1786, 1994.

H. Garbeil and S. K. Rowland, Hawaii Institute of Geophysics and Planetology, School of Ocean and Earth Science and Technology, University of Hawaii, 2525 Correa Rd, Honolulu, HI 96822. (e-mail: scott@pgd.hawaii.edu)